MICROSCOPIC AND ELECTROCHEMICAL CHARACTERIZATION OF ALUMINA CERAMIC FILMS DEVELOPED ONTO 316L STAINLESS STEEL BY MICRO-ARC OXIDATION IN PLASMA ELECTROLYSIS

Elisabeta COACĂ[1], Oana Alice RUSU[2], Alexandru Horia MARIN[3], Lucian VELCIU[4], Maria MIHALACHE[5], Victor Aurel ANDREI[6], Teodor VIŞAN[7]

The objective of this paper was to prepare and characterize alumina coatings developed on AISI 316L stainless steel by aluminizing treatment using micro-arc plasma oxidation in an aqueous solution containing 0.1 M $NaAlO_2$ and 0.05 M NaOH. The obtained films were characterized by SEM microscopy and EDS analysis as well as by Tafel polarization curves and electrochemical impedance spectroscopy. Comparative results for steel samples subjected previously to two different surface pre-treatments (oxidation either by cyclic voltammetry in 0.1 M NaOH or in an autoclave with deionised water) were discussed.

Keywords: aluminium oxide films, micro-arc oxidation in plasma electrolysis, AISI 316L stainless steel, SEM microscopy, potentiodynamic polarization curves, EIS spectroscopy

1. Introduction

The 316L austenitic steel has been already selected as structural material in nuclear power plants that work with the modular reactors having liquid heavy metal as coolant [1], i.e. metallic lead or lead-bismuth eutectic alloy. Although the reactors, for instance SUPERSTAR lead fast reactor, are provided with natural circulation of molten Pb as intermediate coolant in their heat exchangers, there are serious safety problems because such melt exhibits strong erosion-corrosion effect on structural materials. Also, the oxygen content in the coolant and higher working temperature (> 500 ^oC) may produce non-protecting iron oxide (Fe_3O_4) onto the steel surface.

[1] PhD student, Dept. of Inorganic, Physical Chemistry and Electrochemistry, University POLITEHNICA of Bucharest, Romania, e-mail: elisabetaandrei@yahoo.com
[2] PhD, researcher, Institute for Nuclear Research, Mioveni, Piteşti, Romania
[3] PhD, researcher, Institute for Nuclear Research, Mioveni, Piteşti, Romania
[4] Researcher, Institute for Nuclear Research, Mioveni, Piteşti, Romania
[5] PhD, researcher, Institute for Nuclear Research, Mioveni, Piteşti, Romania
[6] PhD, researcher, ELSSA Laboratory SRL, Piteşti, Romania
[7] Professor, Dept. of Inorganic, Physical Chemistry and Electrochemistry, University POLITEHNICA of Bucharest, Romania, e-mail: t_visan@chim.upb.ro

The corrosion of steels can be significantly slowed down by previous formation of protective oxide films. These must be resistant to breakdown by maintaining their thickness and compactness. It was found in the tests performed in the laboratory and industrial facilities that corrosion rate for chromium steels in molten Pb-Bi alloy is in the range of 6–60 mg/(m^2h) at 450–500 °C [1]. It can vary with temperature, coolant flow rate, oxygen content and other parameters. In molten lead, this value is about 0.026 mg/(m^2h) at 600 °C [1].

There is a concern regarding the development of cheap and permissive surface treatments of steels, such as the electrodeposition from ionic liquids, chemical vapor deposition, plasma vapor deposition or thermal spray coating. Applying these treatments can produce superficial structures containing aluminium oxide, which provide corrosion resistance in the specific aggressive environments existing in the cooled lead reactors [2-4]. Another technique is the plasma electrolysis that is a hybrid of conventional electrolysis and atmospheric plasma process. Plasma electrolytic oxidation (PEO) is a surface treatment technology which belongs to the large class of plasma electrolytic deposition [4]. In PEO procedure, the sparks or arc plasma micro-discharges in an aqueous solution are utilized to ionize gaseous media resulting from the solution, such that complex compounds films (Al oxide, usually) are synthesized on the metal surface through the plasma chemical interactions. Adherent ceramic coatings are produced [5-8] thus enhancing hardness and wear resistance, as well as thermal and corrosion resistance, compared with other deposition procedures above mentioned. Both formation of a barrier layer in contact with the electrolyte and characterization of entire coating [9-11], including its corrosion resistance [12-14], were recently described.

In the micro-arc oxidation (MAO), which is a variant of PEO procedure, the coatings grow at the sites of micro discharges by applying high dielectric breakdown voltage. The process uses dc, ac (50–60 Hz) or heteropolar pulsed power [4]. Then, rapid heating and cooling of the coating material facilitate generation of oxides, for instance α-Al_2O_3, which can improve the thermomechanical properties of the coating [15]. The final obtained coatings consist in three layers [16]: first is a 200–500 nm thick barrier layer adjacent to the substrate which has high corrosion resistance; the intermediate dense layer (having microcracks and submicrometric-size pores) provides improved hardness (e.g. 1500–2000 HV, depending on the alloy and treatment conditions); the outer layer contains large cavities and pores and is a good support for sealants and primers in corrosion applications because of its porosity.

The mechanism of coating formation in MAO procedure is not fully explained, although the contributions from anodic oxidation, thermal oxidation and plasma chemical reactions are acknowledged [17-20]. It has been shown that by applying ac power during the micro-arc regime the intermediate layer

deposition commences after the initial 15–20 μm thickness of obtained coating [21, 22]. Many efforts were made [23] for improvement the procedure, for instance by reducing treatment time with increasing coating rates (up to 4–5 μm/min) or decreasing the relatively high costs arising from the high current densities (typically 10–60 A/dm^2) and high *ac* voltages (up to 300–400 V) [21]. Also, there were attempts [24, 25] to reduce the formation voltages to 60–80 V by using concentrated aqueous electrolytes (solutions with >100 g/L KOH and 50–80 g/L silicates, phosphates and aluminates of alkaline metals).

In the case of metallic materials which do not belong to the category of 'valve-metals', such as austenitic stainless steels, various methods can be used to achieve the barrier ceramic layer. An adherent film can be obtained either by an initial deposition of Al or other 'valve metal' (Ti, Zr) onto surface of the steel followed by the process of micro-arc oxidation [26], or direct depositing a porous oxide (Al_2O_3, SiO_2) by decomposition of the electrolyte containing alumina silicates, using micro-arc process [27].

In a previous paper [28] we proved the feasibility of using MAO procedure in 0.1 M $NaAlO_2$ + 0.05 M NaOH aqueous solution for the formation of ceramic-like aluminium oxide films on both 304L and 316L austenitic steels. In this work we present detailed information regarding the characterization of the aluminium oxide film prepared onto AISI 316L steel using the same procedure; results of scanning electron microscopy coupled with energy dispersive X-ray analysis and recording of potentiodynamic polarization curves and electrochemical impedance spectra are reported.

2. Experimental

The AISI 316L steel plates (10 mm × 10 mm × 1 mm) were polished with SiC abrasive paper (1200 mesh) to obtain a fine surface suitable for creating adherent deposits, according to [29]. Prior to any treatment, the samples were washed with distilled water and ethanol. Before micro-arc oxidation (MAO) in plasma, a barrier layer was intended to be prepared by means of a preliminary treatment to obtain an iron oxide (FeO_x) film which does not contain Ni and Cr species. There were tested two types of preliminary treatments. One is an oxidation of the steel substrate at room temperature by cyclic voltammetry [28] producing an oxide film of depleted Ni and Cr, as Diaz et al. have suggested [30]; for this, 20 successive cycles were recorded in 0.1 M NaOH aqueous electrolyte at 5 mV/s scan rate, using a PARSTAT 2273 potentiostat (Princeton Applied Research, USA). The other is the oxidation in demineralized water at 600 °C in an autoclave, which produces a layer of magnetite (tens of microns thick) on the steel substrate; obviously, a long autoclaving time has been necessary for obtaining this increase of the layer thickness. Micro-arc oxidation in plasma of 316L stainless

steel surface was conducted in a two-electrode electrochemical cell containing 500 mL of 0.1 M $NaAlO_2$ and 0.05 M NaOH aqueous solution. The used equipment was a homemade experimental set up using programmable *dc* power supply EA-PS 8400-70, with delivered voltage range of 0-400 V (accuracy of about ±1%) and a current range of 0-15 A under constant voltage conditions. As discussed above, the formation of α-Al_2O_3 ceramic film in MAO procedure is based on the combination of anodic oxidation, spark discharge at high voltage and the local thermal treatment at high temperature. Table 1 illustrates the subsequent carried out treatments and the characterization techniques employed for the steel samples.

Table 1.

The performed treatments and characterization techniques

Sample code	**State of substrate**	**Treatment, parameters**	**Characterization techniques**
E	AISI 316L	Without any treatment	Potentiodynamic polarization and EIS in 0.5 M NaCl solution
D1a	AISI 316L treated by **CV**	**Cyclic voltammetry -** 20 cycles in 0.1 M, NaOH aqueous electrolyte, at 5 mV/s scan rate	EIS in 0.5 M NaCl solution
D1b	AISI 316L treated by **CV** and **MAO**	**MAO** - *dc* power source, 320 V, 10 min, aqueous electrolyte: 0.1 M $NaAlO_2$ + 0.05 M NaOH, $t_{electrolyte}$ < 45 °C	SEM, EDS; Potentiodynamic polarization and EIS in 0.5 M NaCl solution
D2a	AISI 316L treated by **autoclaving**	**Autoclaving** in deionized water, 600°C, 80 days	EIS in 0.5 M NaCl solution
D2b	AISI 316L treated by **autoclaving** and **MAO**	**MAO** - *dc* power source, 320 V, 3 min, aqueous electrolyte: 0.1 M $NaAlO_2$ + 0.05 M NaOH, $t_{electrolyte}$ < 45 °C	SEM, EDS; Potentiodynamic polarization and EIS in 0.5 M NaCl solution

In microscopy investigations the samples were prepared in the metallographic way (by cutting, mounting, grinding and wet polishing using waterproof silicon carbide paper with 120-2400 granulation, according to STAS 4203-74). Scanning electron microscopy (SEM) investigations were carried out with VEGA II LMU TESCAN microscope operating at 30 kV; the device is equipped with three detectors: a detector for secondary electrons, a detector for backscattered electrons and the third detector AXS Bruker for energy dispersive X-ray (EDS) spectrometry.

For corrosion characterization, the test coupons (uncoated and coated) of 1 cm^2 surface area were placed in a glass cell (650 mL) which was filled every time

with freshly aqueous electrolyte (0.5 M NaCl solution). A saturated calomel electrode (SCE) was used as the reference electrode and two connected graphite rods were the auxiliary electrodes. Measurements for potentiodynamic polarization curves (Tafel) and electrochemical impedance spectroscopy (EIS) were performed at room temperature using the same PARSTAT 2273 potentiostat.

Tafel polarization diagrams were recorded with 2 mV/s scan rate as E *vs.* log i dependences, where E is the electrode potential and i the measured current density. The impedance spectra [31] were obtained at open circuit potential with a scan frequency range from 100 kHz to 100 mHz and an *ac* amplitude of 10 mV. In order to obtain quantitative data, the experimental EIS results were simulated with equivalent electrical circuits as appropriate models using ZSimpWin software. For the best fit, models with minimum number of circuit elements were selected. In addition to ohmic resistances (R), instead of pure capacitors the constant phase elements (Q) were introduced in the fitting procedure. To assess the goodness of fit between experimental values and those simulated, the chi-squared test was used with suitably low χ^2 error (usually $\chi^2 < 10^{-4}$). Values up to 5% for the error associated with each element were obtained.

3. Results and discussion

Figs. 1 and 2 show the SEM images (as secondary electron micrographs) and results of EDS analysis (spectra and elemental mapping) obtained from a selected area of the films prepared by micro-arc oxidation on 316L stainless steel.

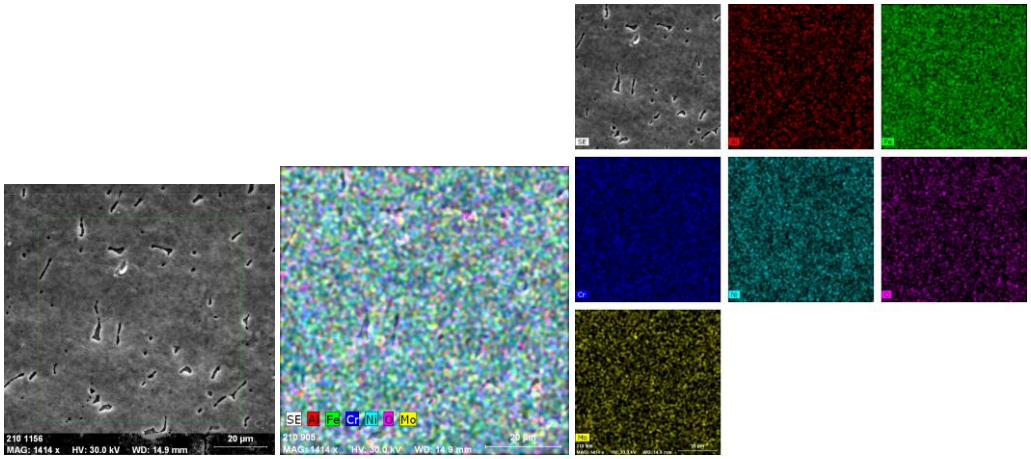

(a) (b) (c)

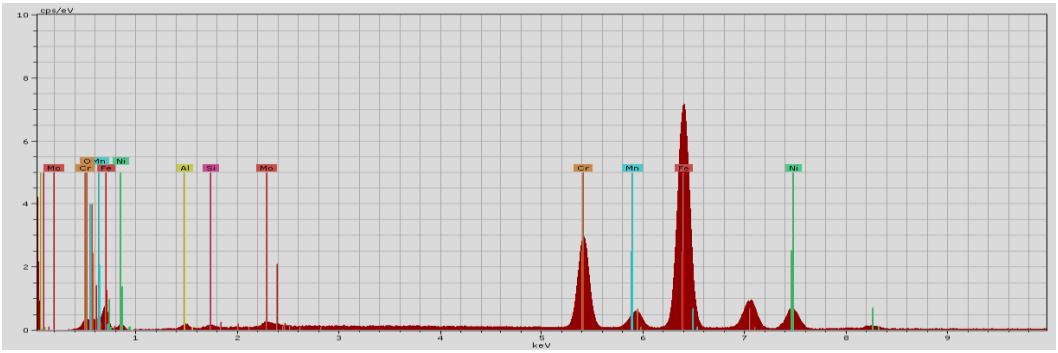

(d)

Fig. 1. SEM +EDS results for **D1b** sample: (a) SEM image, ×1414; (b) chemical map; (c) distribution of separate elements; (d) EDS spectrum.

A SEM elemental mapping provides important information about the uniform distribution of Al, Ni, Fe and Cr which is different for MAO processed samples subjected previously to two different oxidation treatments: cyclic voltammetry (D1b sample) and autoclaving (D2b sample). The chemical composition results determined by EDS in selected area are presented in Table 2.

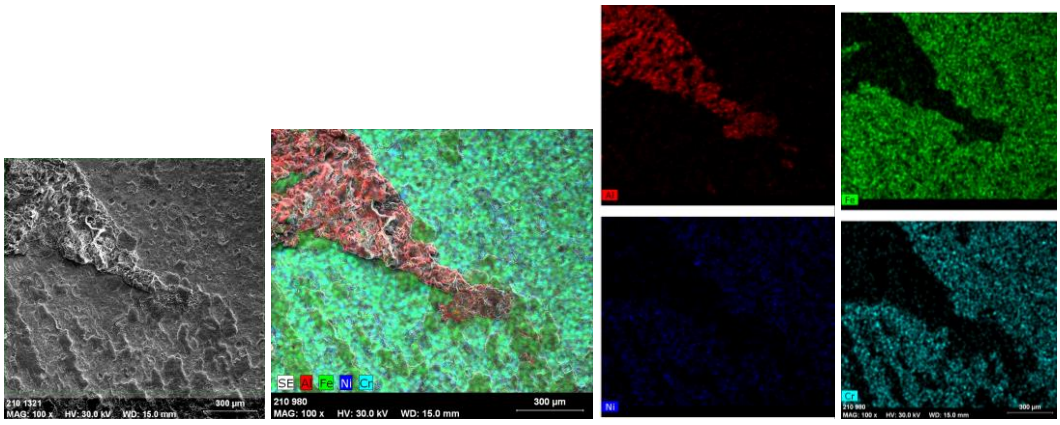

(a) (b) (c)

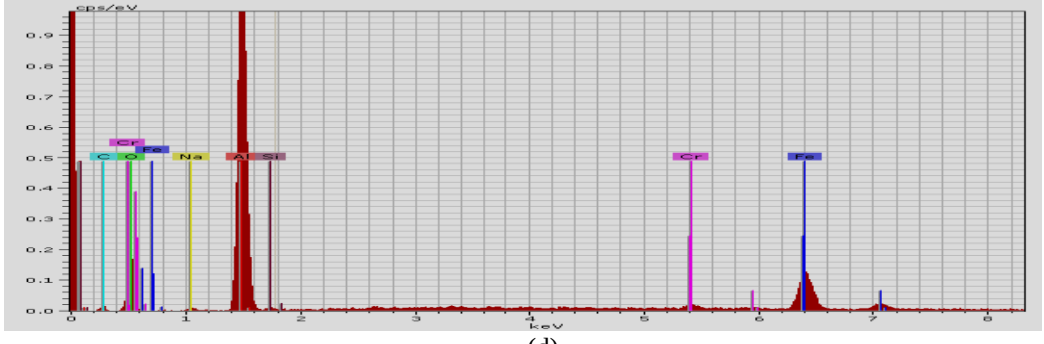

(d)

Fig. 2. SEM + EDS results for **D2b** sample: (a) SEM image, ×100; (b) chemical map; (c) distribution of separate elements; (d) EDS spectrum.

Table 2.

EDS results of the films prepared by micro-arc oxidation on 316L stainless steel subjected previously to two different treatments: cyclic voltammetry (D1b sample) and autoclaving (D2b sample)

Sample	**Concentration** (at%)									
	Al	**Cr**	**Ni**	**Fe**	**Mo**	**Mn**	**Si**	**O**	**C**	**Na**
D1b	1.74	17.25	8.25	63.60	2.80	1.85	0.83	3.68	-	-
D2b	34.65	0.37	-	3.64	-	-	0.10	53.77	7.38	0.09

SEM micrographs for the film on 316L stainless steel successively subjected to cyclic voltammetry and to micro-arc oxidation (D1b sample) had a relatively smooth surface and homogeneous structure, being adherent to the substrate. EDS elemental analysis indicates the presence of a mean content of 1.74 at% Al in the developed layer (a few microns thick). The mean content of Cr (17.25 at%) was not modified comparing with the untreated sample (17.47 at% Cr), this showing that Cr was already stabilized in the structure by cyclic voltammetry. The mean content of Ni (8.25 at%) was decreased comparing with the sample untreated (12.7 at% Ni), a result that is in a good agreement with data previously reported by Diaz *et al*. [30].

SEM micrographs for 316L stainless steel treated by autoclaving and afterwards by MAO plasma electrolysis (D2b sample) showed a leveled and layered structure of film. The inner layer formed by autoclaving consisted in magnetite with a thickness of around 40 μm, while the outer ceramic layer formed by plasma electrolysis had a thickness of around 30 μm. The EDS measurements revealed a heterogeneous chemical composition of the outer layer, consisting in both aluminium oxide and iron oxide; however, the peninsula-like aggregate presented in Figs. 2a-c was predominantly made up of aluminium oxide. The results for D2b sample revealed a mean content of around 35 at% aluminium, a mean content of Cr drastically decreased to 0.37%, while Ni was not present, at all.

Fig. 3 shows comparatively the corrosion behavior of untreated and MAO finally treated samples indicated by potentiodynamic polarization curves as investigation technique. Here the corresponding curves were simply labeled with 316, D1 and D2, respectively. Values of the corrosion potentials E_{corr} and corrosion currents i_{corr} in NaCl aggressive solution were determined from these *E-log i* (electrode potential vs. logarithm of current density) curves as the intercept of the anodic and cathodic Tafel lines at corrosion potential [32].

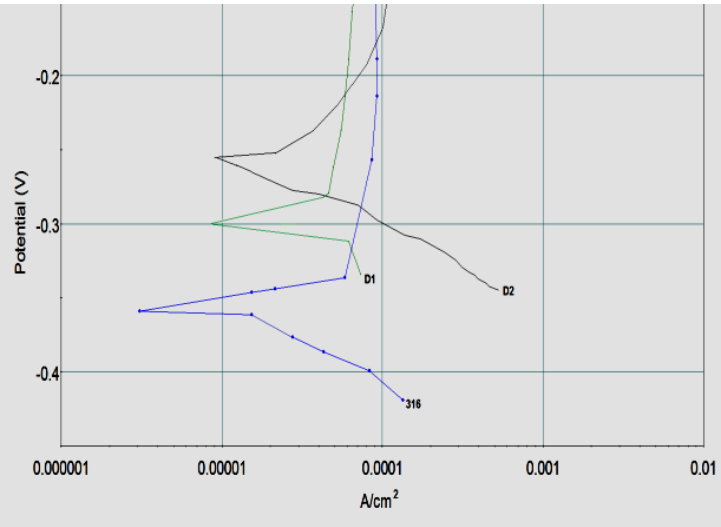

Fig. 3. The Tafel polarization diagrams corresponding to **untreated 316L steel** (curve denoted *316*) as well as MAO treated **D1b** (curve *D1*) and **D2b** (curve *D2*) samples immersed in 0.5 M NaCl solution; scan rate 2 mV/s.

Also, values of corrosion rate v_{corr} expressed as penetration index (mm per year) were evaluated by using Faraday`s number (26.8 A·h), atomic mass of Fe (55.847 g/mole) and density of Fe (7.86 g/cm^3). The results of determining these parameters are presented in Table 3. More positive values of E_{corr} as well as a significant decrease of corrosion rate, lowered by one order of magnitude, can be seen for both MAO treated samples.

Table 3.

Corrosion parameters for untreated and MAO treated samples in 0.5 M NaCl determined from potentiodynamic polarization

Corrosion parameter	Steel samples		
	Untreated AISI 316L (*316* curve)	D1b (*D1* curve)	D2b (*D2 curve*)
E_{corr} (V vs. SCE)	-0.358	-0.300	-0.245
i_{corr} (μA/cm^2)	10.3	1.3	1.1
v_{corr} (mm/year)	0.12	0.015	0.013

EIS measurements were also performed at the open circuit potential in 0.5 M NaCl solution and the obtained impedance spectra were fitted using the ZSimpWin software. Experimental values (discrete points) and fitted curves (solid lines) for Nyquist and Bode impedance spectra of investigated samples (1 cm^2) are represented in Figs. 4-8. Of course, all values of the Bode phase angle in Figs. 4c, 5c, 6c, 7c and 8c are negative. Several time constants appear in these EIS

spectra, indicating the development of different processes. Generally, the simulated and experimental impedance spectra were closely similar.

The proposed equivalent electric circuits for fitting the impedance results are shown in Fig. 9. Rs is the ohmic resistance (uncompensated resistance) of solution. Other resistances, as charge-transfer resistance or resistance of coating should be present in the equivalent circuit, together with capacitors. Instead of pure capacitors the constant phase elements (Q) were introduced; their impedance (Z_Q) is expressed by eq. (1):

$$Z_Q = [Y_o (j\omega)^n]^{-1} \quad (1)$$

where Y_o and n are the specific parameters of Q, $j = \sqrt{-1}$, and ω is the *ac* angular frequency. The exponent n always has subunit values, $n \leq 1$; for n=1 this means that Z_Q is equivalent to a pure capacitance C (Y_o=C), whereas for n=0, Q behaves like a pure ohmic resistance. The numerical results of the fitting procedure are reported in Table 4 indicating the state of steels subjected to different surface treatments and their corrosion.

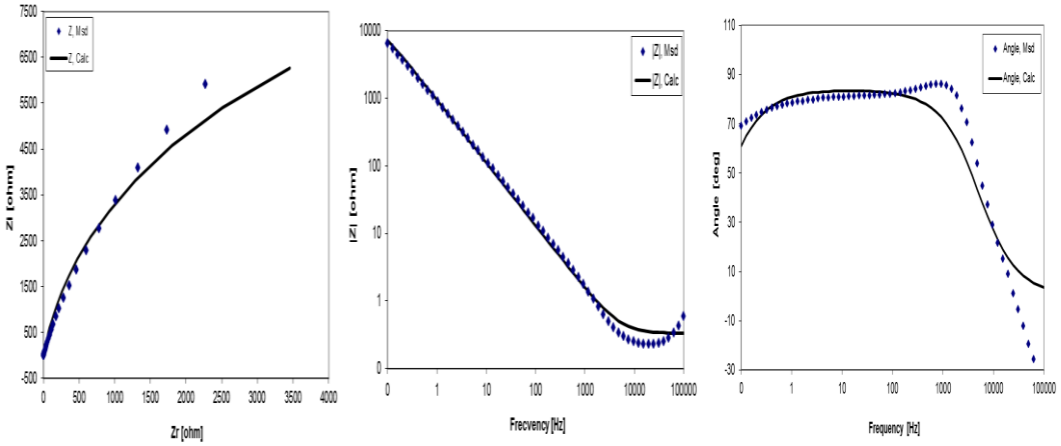

(a) (b) (c)

Fig. 4. Nyquist (a) and Bode (b,c) diagrams for **untreated AISI 316L steel**, 1 cm^2; data fitting with model of Fig.9a

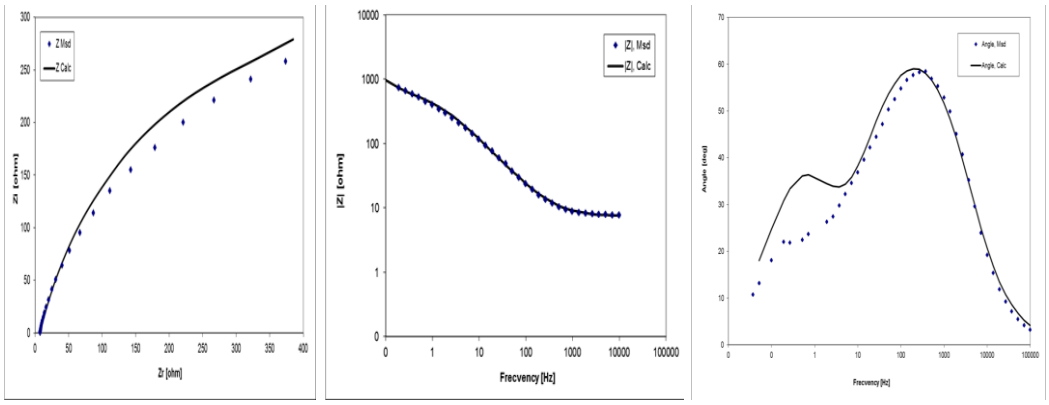

(a) (b) (c)

Fig. 5. Nyquist (a) and Bode (b,c) diagrams for **D1a** sample (model 9b for fitting), 1 cm^2

For untreated sample only, a beginning of a semicircle is recorded in Nyquist plot (Fig. 4a) whereas Bode plots show both impedance modulus vs. *log* frequency as a linear dependence (Fig. 4b) and very negative maximum phase angle, *ca.* -80° (Fig. 4c) within a broad range of frequency. All EIS curves for this sample are characteristic to a simple electrical charging of double layer. The corresponding equivalent circuit (Fig. 9a) indicates a single time constant, as (R(RQ)) model with a parallel combination terms (R1, Q1) in series with the ohmic resistance of the solution (Rs). R1 is here the charge-transfer resistance having the highest values in Table 4 (4445 Ωcm^2), i.e. the lowest corrosion current because the passage of electrons through a double layer is very slowly at the open-circuit potential. Q1 is the constant phase element representing electrochemical double layer with plausible capacity of *ca* 300 $\mu F/cm^2$ and an exponent n=0.88 close to unity (impedance behaving close to an ideal capacitor).

For simply treated by cyclic voltammetry steel sample (D1a), the Nyquist plot shows a beginning of straight line at the end of low-frequency domain (Fig. 5a) thus proving the formation of iron oxides film of depleted Ni and Cr, as above discussed in experimental section. Bode plots show two-time constants. Thus, the impedance modulus (Fig. 5b) at medium frequency represents the response of the coating, while at the low frequency it gives information about processes on the coating/electrolyte interface. Also, the porous FeO_x coating formation is more obvious in Fig. 5c where, by decreasing the frequency, Bode phase angle reached firstly a maximum of -60° followed by a second one at lower frequency. The selected model for fitting is R(QR)(QR) type (Fig. 9b). Comparing to Fig. 9a the equivalent electrical circuit contains supplementary a second parallel combination of R2 and Q2 both representing the coating behavior. R1 and Q1 describe the processes at electrolyte/coating interface whereas R2 and Q2 parameters describe the resistance and capacitance of FeO_x coating.

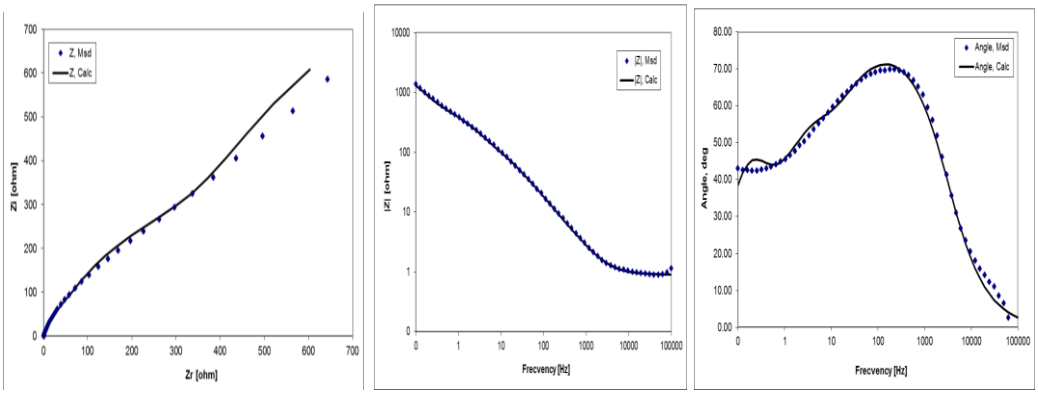

(a) (b) (c)

Fig. 6. Nyquist (a) and Bode (b) diagrams for **D1b** sample (model 9c for fitting), 1 cm^2

As Fig. 6 shows, the impedance plots on D1b sample, obtained after supplementary treatment of D1a with MAO, indicate clearly a formation of a new thicker film at <10 Hz frequencies. In Nyquist diagram (Fig. 6a) the straight line occurring after semicircle is longer and its 45^o slope suggests a porous ceramic coating which allows the diffusion as mass transport of ionic species resulting from corrosion process. In Bode diagram (Fig. 6c), the first maximum of phase angle (-70^o) corresponds to this electric insulator film and the second phase angle maximum is dimmed (but still reaches -40^o) and corresponds to FeO_x film. Fitting these experimental data with R(QR)QR)(QR) type model from Fig. 9c has given the best results. The three-time constants correspond to a series of three parallel circuits. In this model Qp and Rp (letter p comes from the pores of ceramic film) are the components of aluminium oxide ceramic film obtained by MAO, and Q2 and R2 correspond to iron oxide film formed previously by CV.

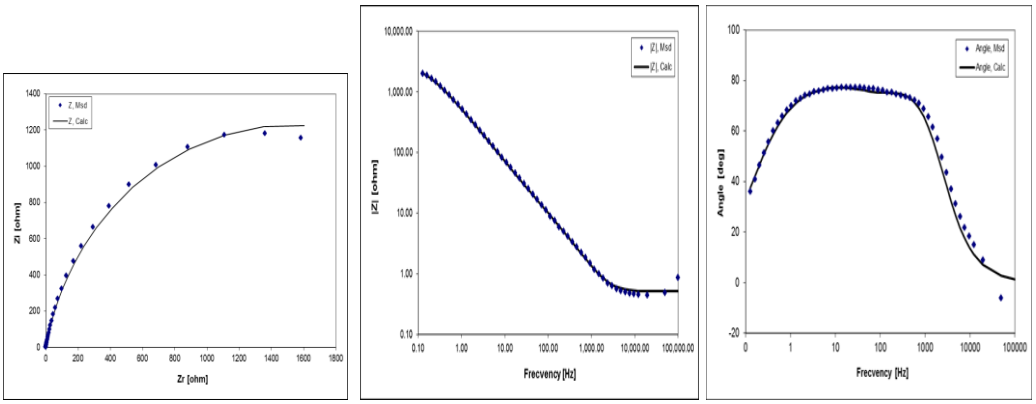

(a) (b) (c)

Fig. 7. Nyquist (a) and Bode (b) diagrams for D2a (model 9d for fitting), 1 cm^2

Although impedance spectra for D2a steel subjected only to autoclaving seem to be somewhat simple, a single Nyquist semicircle in Fig. 7a, a flattened

phase angle maximum of -75° in Fig. 7c, they were heavily modeled. The best results of fitting were obtained with R(Q(R(QR))) equivalent circuit shown in Fig. 9d, in which the resistance of coating (denoted here as Rp) is in series with another parallel circuit related to Q1 of double layer capacitance and R1 – the charge-transfer resistance. In this circuit model, Qp and Rp represent the capacitance and ohmic resistance of the iron oxides film formed by autoclaving.

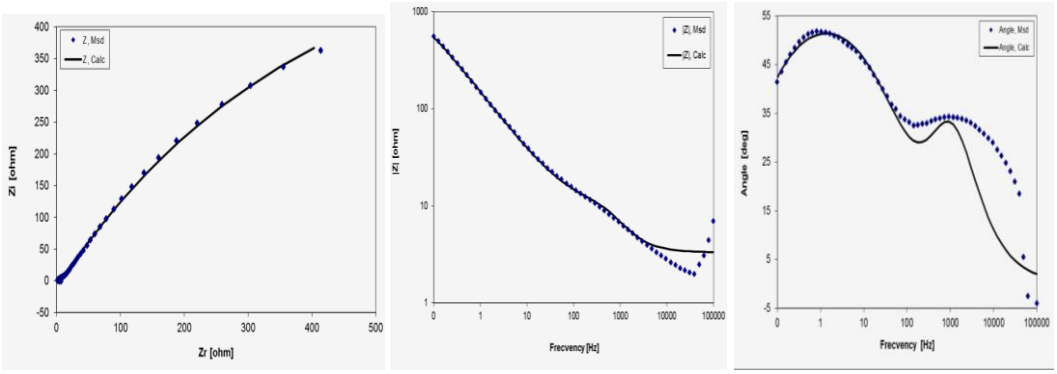

(a) (b) (c)

Fig. 8. Nyquist (a) and Bode (b) diagrams for D2b (model 9c for fitting), 1 cm^2

The experimentally obtained EIS spectra for D2b sample, a steel successively autoclavized and processed by MAO, were also difficult to be interpreted. In Nyquist plot (Fig. 8a) the first semicircle is not at all visible and only the second one is predominant. Also, Bode phase angle vs. frequency curve for D2b (Fig. 8c) has an inverse behavior as D2a sample, because here the maximum at high frequencies has a diminished value (-35°) and the second maximum at low frequencies is more significant, -55°. Thus, we have assigned in this case the R(QR)QR)(QR) model with three-time constants shown in Fig. 9c.

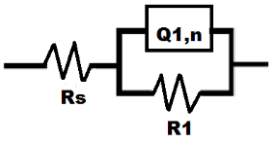

(a)

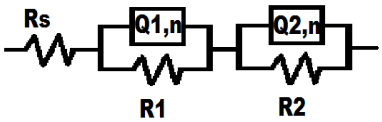

(b)

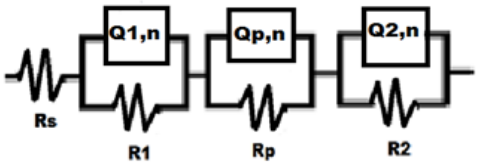

(c)

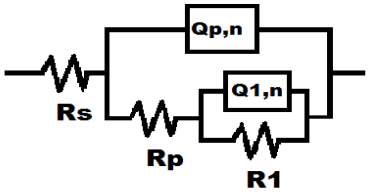

(d)

Fig. 9. Models for the equivalent electrical circuits proposed for fitting the experimental impedance spectra: R(QR) type (a), R(QR)(QR) type (b), R(QR)QR)(QR) type (c) and R(Q(R(QR))) type (d)

It was found that the fitting results of model with three-time constants are suitable to the actual covering process with porous ceramic coating. However, it is observed from Table 4 that charge-transfer resistances (denoted as R1) for both MAO processed samples (D1b, D2b) have not higher values than R1 for simple treated samples (D1a, D2a).

Table 4.

Circuit parameters obtained from fitting the EIS spectra for the samples at open circuit potential immersed in 0.5 M NaCl solution, using the selected equivalent circuits

Sample code	**Rs** (Ω cm^2)	**Q for double layer capacity**		**Charge-transfer resistance** (Ω cm^2)	**Q for FeO_x coating** (obtained by either CV or autoclaving)		**Resistance for FeO_x coating** (Ω cm^2)	**Q for Al_2O_3 ceramic coating**		**Resistance for Al_2O_3 coating** (Ω cm^2)
		Y_0 (μF/cm^2)	**n**		**Y_0** (μF/cm^2)	**n**		**Y_{02}** (μF/cm^2)	**n**	
316L	0.41	304 (**Q1**)	0.88	4445 (**R1**)	-	-	-	-	-	-
D1a	1.43	1100 (**Q1**)	0.77	1927 (**R1**)	5000 (**Q2**)	0.72	59.5 (**R2**)	-	-	-
D1b	5.50	71 (**Q1**)	0.91	1547 (**R1**)	1500 (**Q2**)	1.00	50.5 (**R2**)	35 (**Qp**)	1.00	767 (**Rp**)
D2a	0.51	130 (**Q1**)	1.00	3076 (**R1**)	255 (**Qp**)	0.78	19.3 (**Rp**)	-	-	-
D2b	3.30	41 (**Q1**)	1.00	1456 (**R1**)	1930 (**Q2**)	0.80	3.8 (**R2**)	308 (**Qp**)	1.00	4.3 (**Rp**)

*Symbols for **Q** and **R** in parentheses correspond to the circuit components in Figs. 9

This means that the corrosion currents are not diminished at the open-circuit potential, without negative polarization. Such behavior is typical for a substrate covered with a porous film, exposed to an aggressive electrolytic environment. However, it is expected for the ceramic coating to be more resistant as protective film on AISI 316 steel when it is in contact with liquid lead metal used in the cooled lead nuclear reactors.

4. Conclusions

Alumina ceramic coatings were successfully prepared by micro-arc oxidation (MAO) of 316L stainless steel in $NaAlO_2$ + NaOH solution at temperature < 45°C. The steel was previously covered with iron oxide films by successive voltammetry cycles in NaOH solution or oxidation in demineralized water at 600°C in an autoclave.

Using cyclic voltammetry pre-treatment and subsequent MAO plasma electrolysis, SEM micrographs and EDS analyses of obtained ceramic coating indicated its few microns thickness, and a mixture of oxides of Al, Fe, Cr and Ni; the Cr content remains non-modified comparing with the untreated sample, whereas Fe and Ni contents were decreased. On contrary, SEM/EDS investigations of ceramic coating after autoclaving and subsequent MAO plasma electrolysis showed a layered structure; the inner layer is almost entirely magnetite oxide, but the outer layer has a heterogeneous chemical composition consisting in aluminium oxide (predominantly), iron oxides and traces of chromium oxide.

The comparison of covered ceramic coating steel with un-treated steel made using Tafel potentiodynamic polarization technique in NaCl solution shows the passivation, indicated by more positive corrosion potential and significant decrease of corrosion rate by one order of magnitude. This good corrosion protection behavior may be explained by long time duration of this kind of experiments that allow the formation of a protective layer of corrosion products.

Electrochemical impedance spectroscopy (EIS) response in NaCl solution of alumina ceramic films developed on 316L stainless steel by micro-arc oxidation after either voltammetric cycling or autoclaving, as pre-treatments, matches very well with theoretical model of equivalent electrical circuit characteristic to the substrat / porous film / electrolyte systems. Moreover, there was a good correlation between the EIS experimental and fitted results and the scanning electron microscopy (SEM/EDS) investigation.

Overall, the measurements confirm the development of a porous ceramic coating on 316L austenitic steel by performing complex treatments, including substrate modification and plasma electrolytic oxidation.

R E F E R E N C E S

[1]. ***, Liquid Metal Coolants for Fast Reactors Cooled by Sodium, Lead, and Lead-Bismuth Eutectic, IAEA Nuclear Energy Series, Technical Report No. NP-T-1.6, IAEA, Vienna, 2012

[2]. *J. Konys, W. Krauss, N. Holstein*, Development of advanced Al coating process for future applications as anti-corrosion and T-permeation barriers, Fusion Eng. Design, **vol. 85**, 2010, pp. 2141-2145.

[3]. *R. Sitek, J. Kaminski, P. Sallot, K.J. Kurzydlowski*, Structure and properties of iron aluminide layers fabricated by the chemical vapour deposition on 316L steel, Mater. Sci.-Poland, **vol. 28** (1), 2010, pp. 163-172.

[4]. *A.L.Yerokhin, X. Nie, A. Leyland, A. Matthews, S.J. Dowey*, Plasma electrolysis for surface engineering, Surf. Coat. Technol., **vol. 122**, 1999, pp. 73–93.

[5]. *A.L. Yerokhin, L.O. Snizhko, N.L. Gurevina, A. Leyland, A. Pilkington, A. Matthews*, Spatial characteristics of discharge phenomena in plasma electrolytic oxidation of aluminium alloy, Surf. Coat. Technol., **vol. 177-178**, 2004, pp. 779–783.

[6]. *W. Gu, D. Shen, Y. Wang, G. Chen, W. Feng, G. Zhang, S. Fan, C. Liu, S. Yang*, Deposition of duplex Al_2O_3/aluminium coatings on steel using a combined technique of arc spraying and plasma electrolytic oxidation, Appl. Surf. Sci., **vol. 252** (8), 2006, pp. 2927-2932

[7]. *E.V. Parfenov, A. L. Yerokhin, A. Matthews*, Frequency response studies for the plasma electrolytic oxidation process, Surf. Coat. Technol., **vol. 201** (21), 2007, pp. 8661–8670.

[8]. *E. Matykina , R. Arrabal, P. Skeldon, G.E. Thompson*, Investigation of the growth processes of coatings formed by AC plasma electrolytic oxidation of aluminium, Electrochim. Acta, **vol. 54** (27), 2009, pp. 6767–6778.

[9]. *R. Arrabal, M. Mohedano, E. Matykina, A. Pardo, B. Mingo, M.C. Merino*, Characterization and wear behaviour of PEO coatings on 6082-T6 aluminium alloy with incorporated α-Al_2O_3 particles, Surf. Coat. Technol., **vol. 269**, 2015, pp. 64-73.

[10]. *V. Dehnavi, B.L. Luan, X.Y. Liu, D.W. Shoesmith, S. Rohani*, Correlation between plasma electrolytic oxidation treatment stages and coating microstructure on aluminium under unipolar pulsed DC mode, Surf. Coat. Technol., **vol. 269**, 2015, pp. 91-99.

[11]. *A.E. Gulec, Y. Gencer, M. Tarakci*, The characterization of oxide based ceramic coating synthesized on Al–Si binary alloys by microarc oxidation, Surf. Coat. Technol., **vol. 269**, 2015, pp. 100-107.

[12]. *H. Deng, Z. Ma, X. Zhang, Y. Zhang, X. Liu*, Corrosion resistance in simulated DMFC environment of plasma electrolytic oxidation coating prepared on aluminium alloy, Surf. Coat. Technol., **vol. 269**, 2015, pp. 108-113.

[13]. *F. Muhaffel, F. Mert, H. Cimenoglu, D. Höche, M.L. Zheludkevich, C. Blawert*, Characterisation and corrosion behaviour of plasma electrolytic oxidation coatings on high pressure die cast Mg–5Al–0.4Mn–xCe (x = 0, 0.5, 1) alloys, Surf. Coat. Technol., **vol. 269**, 2015, pp. 200-211.

[14]. *M. Mohedano, E. Matykina, R. Arrabal, B. Mingo, M.L. Zheludkevich*, PEO of rheocast A356 Al alloy: energy efficiency and corrosion properties, Surf. Interface Anal., **vol. 48** (8), 2016, pp. 953-959.

[15]. *E. Matykina, R. Arrabal, P. Skeldon, G. E. Thompson*, Optimisation of the plasma electrolytic oxidation process efficiency on aluminium, Surf. Interface Anal., **vol. 42** (4), 2010, pp. 221–226.

[16]. *E. Matykina, R. Arrabal, P. Skeldon, G. E. Thompson*, Incorporation of zirconia nanoparticles into coatings formed on aluminium by AC plasma electrolytic oxidation, J. Appl. Electrochem., **vol. 38** (10), 2008, pp. 1375–1383.

[17]. *W. Xue, Z. Deng, R. Chen, T. Zhang*, Growth regularity of ceramic coatings formed by microarc oxidation on Al–Cu–Mg alloy, Thin Solid Films, **vol. 372** (1-2), 2000, pp. 114–117.

[18]. *G. Sundararajan, L. Rama Krishna*, Mechanisms underlying the formation of thick alumina coatings through the MAO coating technology, Surf. Coat. Technol., **vol. 167** (2–3), 2003, pp. 269–277.

[19]. *Y. Yan, Y. Han, J. Huang*, Formation of Al_2O_3–ZrO_2 composite coating on zirconium by micro-arc oxidation, Scripta Mater., **vol. 59** (2), 2008, pp. 203–206.

[20]. *Y. Yürektürk, F. Muhaffel, M. Baydoğan*, Characterization of micro arc oxidized 6082, aluminium alloy in an electrolyte containing carbon nanotubes, Surf. Coat. Technol., **vol. 269**, 2015, pp. 83-90.

[21]. *F. Jaspard-Mecuson, T. Czerwiec, G. Henrion, T. Belmonte, L. Dujardin, A. Viola, J. Beauvir*, Tailored aluminium oxide layers by bipolar current adjustment in the Plasma Electrolytic Oxidation (PEO) process, Surf. Coat. Technol., **vol. 201** (21), 2007, pp. 8677–8682.

[22]. *A.I. Sonova, O.P. Terleeva*, Morphology, structure, and phase composition of microplasma coatings formed on Al-Cu-Mg alloy, Prot. Met., **vol. 44** (1), 2008, pp 65–75.

[23]. *A.L. Yerokhin, A. Shatrov, V. Samsonov, P. Shashkov, A. Pilkington, A. Leyland, A. Matthews*, Oxide ceramic coatings on aluminium alloys produced by a pulsed bipolar plasma electrolytic oxidation process, Surf. Coat. Technol., **vol. 199** (2-3), 2005, pp. 150–157.

[24]. *S.-H. Deng, D.-Q. Yi, Z.-Q. Gong, Y.-C. Su*, Influence of potential on the structure and properties of microarc oxidation coating on Mg alloy, Anti-Corros. Methods Mater., **vol. 55** (5), 2008, pp. 264-269.

[25]. *M. Aliofkhazraei, A.S. Rouhaghdam*, Fabrication of Nanostructures by Plasma Electrolysis, chapter 8: Nanostructured coatings made by Plasma Electrolytic Oxidation, Wiley-VCH, Weinheim, 2010, pp. 211.

[26]. *Z. Wu, Y. Xia, G. Li, F. Xu*, Structure and mechanical properties of ceramic coatings fabricated by plasma electrolytic oxidation on aluminized steel, Appl. Surf. Sci., **vol. 253** (20), 2007, pp. 8398–8403.

[27] *S.A. Karpushenkov, G.L. Shchukin, A.L. Belanovich, V.P. Savenko, A.I. Kulak*, Plasma electrolytic ceramic-like aluminium oxide coatings on iron, J. Appl. Electrochem., **vol. 40**, 2010, pp. 365–374.

[28]. *V.A. Andrei, E. Coaca, M. Mihalache, V. Malinovschi, M. Patrascu-Minca*, Study of thin films developed during the electrochemical engineering techniques based on Plasma Electrolytic Oxidation applied on austenitic steels, Surf. Interface Anal., **vol. 48** (7), 2016, pp. 654-659.

[29]. *G.F. Vander Voort (Ed.)*, ASM Handbook, Volume 9: Metallography and Microstructures, ASM International, Materials Park, Ohio, 2004.

[30]. *B. Díaz, L. Freire, M.F. Montemor, X R. Novoa*, Oxide film growth by CSV on AISI 316L: a combined electrochemical and analytical characterization, J. Braz. Chem. Soc., **vol. 24** (8), 013, pp. 1246-1258.

[31]. *A. Fattah-alHosseini, S. Taheri Shoja, B. Heydari Zebardast, P. Mohamadian Samim*, An electrochemical impedance spectroscopic study of the passive state on AISI 304 stainless steel, Int. J. Electrochem., **vol. 2011**, 2011, Article ID 152143.

[32]. *I. Szatmári, L.M. Tudosie, A. Cojocaru, M. Lingvay, P. Prioteasa, T. Visan*, Studies on biocorrosion of stainless steel and copper in Czapek Dox medium with Aspergillus niger filamentous fungus, UPB Sci. Bull. Series B, **vol. 77** (3), 2015, pp. 91-102.